A Modified Tolles–Lawson Model Robust to the Errors of the Three-Axis Strapdown Magnetometer

Qi Han, Zhenjia Dou, Xiaojun Tong, Xiang Peng, and Hong Guo

***Abstract*— The estimating of the Tolles–Lawson model's coefficients plays an important role in aeromagnetic compensation. The directional cosines, which are indispensable for estimating the coefficients, are usually measured by a three-axis strapdown magnetometer in a general aeromagnetic survey system. However, in some cases, the scalar magnetometer may have a much higher accuracy than the three-axis strapdown magnetometer. This imbalance of the measurement accuracy is then introduced into the Tolles–Lawson model and affects the estimation of the coefficients. In this letter, a modified Tolles–Lawson model is introduced to reduce the imbalance through substituting the error model of the three-axis strapdown magnetometer into the calculation of the directional cosines. The characteristics of the modified model are analyzed and the corresponding coefficient-estimating system is developed. Simulation results illustrate that the modified model is more robust to the larger errors of the three-axis strapdown magnetometer than the classical model.**

***Index Terms*— Aeromagnetic compensation, magnetometer, regression analysis, Tolles–Lawson model.**

I. Introduction

AEROMAGNETIC measurement has been widely applied in geological studies, mineral exploration, and magnetic anomaly detection for decades [1]–[3]. In practice, the magnetic interference related to aircraft maneuvers should be eliminated from the output signal of the magnetometer, which is usually accomplished by the so-called aeromagnetic compensation.

The aircraft magnetic interference can be modeled as a function of the cosines of the direction angles formed by the geomagnetic field with the natural axes of the aircraft [4]. Through estimating the unknown coefficients of the Tolles–Lawson model in advance, the aircraft magnetic interference during an actual aeromagnetic survey can be evaluated and eliminated in real time. It can be seen that both the magnetometer and the coefficient-estimating method play crucial roles in aeromagnetic compensation. Researchers have achieved much progresses in different aspects of this field, such as sensors [5]–[7], modeling and analysis [8]–[10], parameter estimation [11]–[20], system implementation [21]–[28], and so on. Commercial systems are also available from a number of companies [3]. Nonetheless, with the increasing demand for measurement accuracy, it is still necessary to develop and improve the relevant techniques.

Manuscript received June 17, 2016; revised October 31, 2016; accepted November 28, 2016. Date of publication January 16, 2017; date of current version February 23, 2017. This work was supported in part by the National Natural Science Foundation of China under Grant 61301099, Grant 61471141, Grant 61361166006, and Grant 61201399 and in part by the Fundamental Research Funds for the Central Universities under Grant HIT.KISTP.201414.

Q. Han, Z. Dou, and X. Tong are with the School of Computer Science and Technology, Harbin Institute of Technology, Harbin 150001, China (e-mail: qi.han@hit.edu.cn).

X. Peng and H. Guo are with the School of Electronics Engineering and Computer Science, Peking University, Beijing 100871, China.

Color versions of one or more of the figures in this letter are available online at http://ieeexplore.ieee.org.

Digital Object Identifier 10.1109/LGRS.2016.2640188

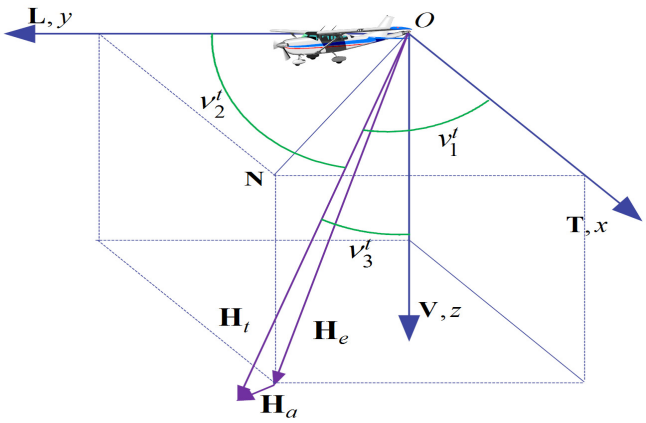

Fig. 1. Reference system used in aeromagnetic compensation.

In practice, the directional cosines are usually calculated using the outputs of a three-axis strapdown magnetometer, while the total field intensities are measured with a proton or optical-pumping scalar magnetometer. Generally, the three-axis strapdown magnetometer is subjected to the errors of the null-shift, the nonorthogonality, the misalignment, the measurement noise, and so on, which can lead to geomagnetic vector measurement errors of about hundreds of nanotesla [29]. Thus, in some cases, the scalar magnetometer may have a higher accuracy than the three-axis strapdown magnetometer. As a result, the accuracy of the obtained directional cosines may not be matched with that of the measured total field intensities. However, both the obtained directional cosines and the measured total field intensities should be put into the Tolles–Lawson model, which inevitably brings imbalance into the system of linear equations established to estimate the coefficients. This imbalance and its influences on the estimation of the coefficients have not been given much attention so far as is known to the authors. The work presented in this letter substitutes the error model of the three-axis strapdown magnetometer into the calculation of the directional cosines and then derives a modified Tolles–Lawson model. Thus, the imbalance between the two kinds of magnetometers can be reduced.

II. Modified Tolles–Lawson Model

The reference system used in this letter is defined by the transverse, longitudinal, and vertical axes of the aircraft with the scalar magnetometer located at the origin O, as shown

in Fig. 1. The axes of the three-axis strapdown magnetometer coincide with the ones of the reference system. The total field $\mathbf{H}_t$ is the vector sum of the geomagnetic field $\mathbf{H}_e$ and the aircraft magnetic interference $\mathbf{H}_a$. The geomagnetic north is denoted by $\mathbf{N}$.

According to the Tolles–Lawson model, the aircraft magnetic interference includes the permanent, the induced, and the eddy-current components and its projection on $\mathbf{H}_t$ can be expressed as

$$H_{at} = \mathbf{P}\mathbf{u}_t + \mathbf{u}_t^T\mathbf{A}\mathbf{u}_t + \left(\mathbf{u}_t^T\right)'\mathbf{B}\mathbf{u}_t \tag{1}$$

where $\mathbf{P}$, $\mathbf{A}$, and $\mathbf{B}$ stand for the unknown coefficient matrices defined in the following:

$$\mathbf{P} = (p_1 \quad p_2 \quad p_3) \tag{2}$$

$$\mathbf{A} = \begin{pmatrix} a_{11} & a_{12} & a_{13} \\ a_{21} & a_{22} & a_{23} \\ a_{31} & a_{32} & a_{33} \end{pmatrix} \tag{3}$$

$$\mathbf{B} = \begin{pmatrix} b_{11} & b_{12} & b_{13} \\ b_{21} & b_{22} & b_{23} \\ b_{31} & b_{32} & b_{33} \end{pmatrix} \tag{4}$$

and the vector $\mathbf{u}_t$ is the column vector consisting of the directional cosines of the angles $v_i^t (i = 1, 2, 3)$ formed by $\mathbf{H}_t$ with the **x**-, **y**- and **z**-axes, respectively, and can be given by

$$\mathbf{u}_t = \mathbf{H}_t / \|\mathbf{H}_t\|. \tag{5}$$

In practice, the three elements of $\mathbf{H}_t$ can be measured with the three-axis strapdown magnetometer and the value of $\|\mathbf{H}_t\|$ can be obtained with the output of the scalar magnetometer.

In order to calculate and subtract H_{at} from the measured total field intensity $\|\mathbf{H}_t\|$, the elements of $\mathbf{P}$, $\mathbf{A}$, and $\mathbf{B}$ need to be determined, using the direction cosines $\mathbf{u}_t$ and the system of equations in (1). It is obvious that the accuracy of the calculated $\mathbf{u}_t$ is important to the estimation of the coefficients, and hence, the error characteristics of the three-axis strapdown magnetometer should be taken into consideration.

As derived in [6], the output vector $\mathbf{H}_m$ of the three-axis strapdown magnetometer can be described as

$$\mathbf{H}_m = \mathbf{C}\mathbf{H}_t + \boldsymbol{l} + \boldsymbol{n} \tag{6}$$

where $\boldsymbol{n} \in \mathbb{R}^3$ denotes the Gaussian wideband noise, $\boldsymbol{l} \in \mathbb{R}^3$ denotes the null-shift error, and $\mathbf{C} = \mathbf{C}_S\mathbf{C}_O\mathbf{C}_L$ with $\mathbf{C}_S \in \mathbb{R}^{3\times3}$, $\mathbf{C}_O \in \mathbb{R}^{3\times3}$, and $\mathbf{C}_L \in \mathbb{R}^{3\times3}$ denoting the errors from the scale factor, the nonorthogonality, and the misalignment with respect to the axes of the aircraft, respectively. Besides, the simplicity of (6) makes it flexible to model other external factors conforming to it. It needs to be emphasized that the environmental errors, such as the soft iron error and the hard iron error, are not expressed explicitly in (6), because they have been contained in $\mathbf{H}_t$.

If we assume that the inverse of $\mathbf{C}$ exists and denote it as $\mathbf{M}$, then $\mathbf{H}_t$ can be recast as

$$\mathbf{H}_t = \mathbf{M}\mathbf{H}_m - \mathbf{M}\boldsymbol{l} - \mathbf{M}\boldsymbol{n}. \tag{7}$$

Thus, if (7) is substituted into (5), $\mathbf{u}_t$ can be rewritten as

$$\mathbf{u}_t = \lambda\mathbf{M}\mathbf{u}_m - \mathbf{M}\mathbf{s}_m \tag{8}$$

where $\mathbf{u}_m = \mathbf{H}_m / \|\mathbf{H}_m\|$, $\mathbf{s}_m$ and λ are defined as follows:

$$\lambda = \|\mathbf{H}_m\| / \|\mathbf{H}_t\| = \|\mathbf{C}\mathbf{H}_t + \boldsymbol{l} + \boldsymbol{n}\| / \|\mathbf{H}_t\| \tag{9}$$

$$\mathbf{s}_m = (\boldsymbol{l} + \boldsymbol{n}) / \|\mathbf{H}_t\|. \tag{10}$$

By substituting (8) into (1), we arrive at the following:

$$\begin{aligned} H_{at} = {} & \lambda\mathbf{P}_M\mathbf{u}_m + \lambda^2\mathbf{u}_m^T\mathbf{A}_M\mathbf{u}_m + \lambda^2\left(\mathbf{u}_m^T\right)'\mathbf{B}_M\mathbf{u}_m - \mathbf{P}_M\mathbf{s}_m \\ & + \mathbf{s}_m^T\mathbf{A}_M\mathbf{s}_m + \left(\mathbf{s}_m^T\right)'\mathbf{B}_M\mathbf{s}_m - \lambda\mathbf{u}_m^T\mathbf{A}_M\mathbf{s}_m - \lambda\mathbf{s}_m^T\mathbf{A}_M\mathbf{u}_m \\ & - \lambda\left(\mathbf{u}_m^T\right)'\mathbf{B}_M\mathbf{s}_m - \lambda\left(\mathbf{s}_m^T\right)'\mathbf{B}_M\mathbf{u}_m \end{aligned} \tag{11}$$

where $\mathbf{P}_M$, $\mathbf{A}_M$, and $\mathbf{B}_M$ are given by

$$\mathbf{P}_M = \mathbf{P}\mathbf{M}, \quad \mathbf{A}_M = \mathbf{M}^T\mathbf{A}\mathbf{M}, \quad \mathbf{B}_M = \mathbf{M}^T\mathbf{B}\mathbf{M}. \tag{12}$$

If we define τ_s as follows:

$$\begin{aligned} \tau_s = {} & -\mathbf{P}_M\mathbf{s}_m + \mathbf{s}_m^T\mathbf{A}_M\mathbf{s}_m + \left(\mathbf{s}_m^T\right)'\mathbf{B}_M\mathbf{s}_m - \lambda\mathbf{u}_m^T\mathbf{A}_M\mathbf{s}_m \\ & - \lambda\mathbf{s}_m^T\mathbf{A}_M\mathbf{u}_m - \lambda\left(\mathbf{u}_m^T\right)'\mathbf{B}_M\mathbf{s}_m - \lambda\left(\mathbf{s}_m^T\right)'\mathbf{B}_M\mathbf{u}_m \end{aligned} \tag{13}$$

and put it into (11), the modified Tolles–Lawson model can be given by

$$H_{at} = \lambda\mathbf{P}_M\mathbf{u}_m + \lambda^2\mathbf{u}_m^T\mathbf{A}_M\mathbf{u}_m + \lambda^2\left(\mathbf{u}_m^T\right)'\mathbf{B}_M\mathbf{u}_m + \tau_s. \tag{14}$$

The major difference of (14) from (1) in terms of mathematical form is the introduction of the factor λ and the additional term τ_s, illuminating the imbalance between the scalar magnetometer and the three-axis strapdown magnetometer. The value of λ can be determined directly according to (9), but it is not so straightforward for τ_s.

Without loss of generality, (14) can be rewritten as

$$H_{at} = \lambda\sum_{i=1}^{3}\bar{p}_i\bar{u}_i + \lambda^2\sum_{i=1}^{3}\sum_{j=1}^{3}(\bar{a}_{ij}\bar{u}_i\bar{u}_j + \bar{b}_{ij}(\bar{u}_i)'\bar{u}_j) + \tau_s \tag{15}$$

where $\bar{p}_i$, $\bar{a}_{ij}$, $\bar{b}_{ij}$, and $\bar{u}_i$ denote the elements of $\mathbf{P}_M$, $\mathbf{A}_M$, $\mathbf{B}_M$, and $\mathbf{u}_m$, respectively. For the sake of convenience, (15) can be described in vector form as an inner product

$$H_{at} = \boldsymbol{\delta}\boldsymbol{\theta} + \tau_s \tag{16}$$

where $\boldsymbol{\delta}$ denotes the row vector constructed by $\lambda\bar{u}_i$, $\lambda\bar{u}_i\bar{u}_j$, and $\lambda(\bar{u}_i)'\bar{u}_j$, and $\boldsymbol{\theta}$ denotes the corresponding column vector consisting of $\bar{p}_i$, $\bar{a}_{ij}$, and $\bar{b}_{ij}$.

III. Coefficient-Estimating System

By defining the projection of the geomagnetic field $\mathbf{H}_e$ on the total magnetic field $\mathbf{H}_t$ as H_{et}, we obtain the following:

$$\|\mathbf{H}_t\| = H_{at} + H_{et} = \boldsymbol{\delta}\boldsymbol{\theta} + \tau_s + H_{et}. \tag{17}$$

In order to estimate $\boldsymbol{\theta}$, the equation group of (17) can be established as follows:

$$\mathbf{H} = \boldsymbol{\Delta}\boldsymbol{\theta} + \Gamma_s + \mathbf{H}_{et} \tag{18}$$

where $\mathbf{H}$, Γ_s, and $\mathbf{H}_{\text{et}}$ denote the column vectors composed by the values of $\|\mathbf{H}_t\|$, τ_s, and H_{et}, respectively, and $\boldsymbol{\Delta}$ denotes the matrix constructed by the corresponding $\boldsymbol{\delta}$ at each sampling point.

Unlike $\mathbf{H}$ and $\mathbf{\Delta}$, $\mathbf{H}_{\text{et}}$ and Γ_s cannot be obtained directly from any sensors so that they must be removed before estimating the coefficient vector $\boldsymbol{\theta}$. Considering the frequency range of the aircraft maneuvers, in general, a bandpass finite impulse response (FIR) filter *bpf* can be applied to (18)

$$bpf(\mathbf{H}) = bpf(\mathbf{\Delta})\boldsymbol{\theta} + bpf(\Gamma_s) + bpf(\mathbf{H}_{et}) \tag{19}$$

where $bpf(\boldsymbol{\chi})$ returns the filtered result of vector $\boldsymbol{\chi}$ or each column of $\boldsymbol{\chi}$ if it is a matrix. Herein, both $\mathbf{H}_{et}$ and Γ_s are supposed to be $\mathbf{0}$ in the passband of *bpf*

$$bpf(\mathbf{H}_{et}) = \mathbf{0} \quad bpf(\Gamma_s) = \mathbf{0}. \tag{20}$$

Then, the coefficient vector $\boldsymbol{\theta}$ can be estimated based on the following equation:

$$bpf(\mathbf{H}) = bpf(\mathbf{\Delta})\boldsymbol{\theta} \tag{21}$$

using regression techniques. Unfortunately, the assumption (20) is usually unsatisfied in practice. In some cases, the component of the geomagnetic field in the filtered magnetic field signal, i.e., $bpf(\mathbf{H}_{et})$, cannot be ignored due to the geomagnetic gradient. In practice, it can be modeled as follows [30]:

$$bpf(\mathbf{H}_{et}) = e_1 \cdot bpf(\mathbf{Q}) + e_2 \cdot bpf(\boldsymbol{R}) + e_3 \cdot bpf(\mathbf{D}) \tag{22}$$

where $\mathbf{Q}$, $\boldsymbol{R}$, and $\mathbf{D}$ denote the longitude, latitude, and altitude of the aircraft, and $e_i (i = 1, 2, 3)$ denote the corresponding unknown coefficients. Therefore, (19) can be rewritten as

$$bpf(\mathbf{H}) = bpf(\mathbf{\Delta}_C)\boldsymbol{\eta} + bpf(\Gamma_s) \tag{23}$$

where $\mathbf{\Delta}_C = (\mathbf{\Delta}\ \mathbf{Q}\ \boldsymbol{R}\ \mathbf{D})$ and $\boldsymbol{\eta} = (\boldsymbol{\theta}\ e_1\ e_2\ e_3)^T$. According to the regression theory, the characteristics of $bpf(\mathbf{\Delta}_C)$ and $bpf(\Gamma_s)$ play an important role in estimating $\boldsymbol{\eta}$.

As a matter of fact, the multicolinearity of $bpf(\mathbf{\Delta}_C)$ is a well-known problem which has been studied for decades in aeromagnetic compensation [11], [16]–[18]. The multicolinearity of $bpf(\mathbf{\Delta}_C)$ stems from the restricted aircraft maneuvers. In order to estimate the coefficients, the aircraft is required to perform the so-called calibration flight, including a series of maneuvers, such as rolls, pitches, and yaws in four orthogonal headings [31]. However, the aircraft cannot alter the dip angle [11] so that the magnetic field data collected during the calibration flight are incomplete to determine the true coefficients. Besides, the filter *bpf* also has an impact on the multicolinearity [18]. Many methods have been studied to address this type of ill-posed linear inverse problem for decades [32]–[34]. Practically, the estimator based on ridge regression analysis is demonstrated to be able to permit useful and stable compensation results [26].

According to (13), $bpf(\Gamma_s)$ can hardly be determined directly. From the view of the conventional linear regression model, the elements of $bpf(\Gamma_s)$ are generally assumed to be independent and have a common variance, for instance, obeying the standard normal distribution $N(0, 1)$. However, this is seldom fully satisfied in practice. On the contrary, the elements of $bpf(\Gamma_s)$ have autocorrelation and heteroscedasticity, which are mainly caused by the following reasons. First, the measured geomagnetic field intensity $\|\mathbf{H}_t\|$ in (10) implies the autocorrelation of $\mathbf{s}_m$ which is to be substituted into (13). Second, the direction cosine $\mathbf{u}_m$ in the last four terms of (13) varies with the aircraft maneuvers and to some extent, would be autocorrelated. Thus, the autocorrelation of τ_s can be demonstrated according to (13). Furthermore, the convolution operation of the bandpass FIR filter would also lead to the autocorrelation of $bpf(\Gamma_s)$. Similarly, the heteroscedasticity of $bpf(\Gamma_s)$ can be analyzed. The generalized least-square method is usually adopted to deal with the autocorrelation and heteroscedasticity.

For convenience, (23) is rewritten as follows:

$$\mathbf{Y} = \mathbf{X}\boldsymbol{\eta} + \boldsymbol{\xi} \tag{24}$$

where $\mathbf{Y} = bpf(\mathbf{H})$, $\mathbf{X} = bpf(\mathbf{\Delta}_C)$, and $\boldsymbol{\xi} = bpf(\Gamma_s)$. Ideally, the generalized least-square solution is given by

$$\boldsymbol{\eta}_{gls} = (\mathbf{X}^T\mathbf{V}^{-1}\mathbf{X})^{-1}\mathbf{X}^T\mathbf{V}^{-1}\mathbf{Y} \tag{25}$$

where $\mathbf{V}$ denotes the covariance matrix of $\boldsymbol{\xi}$. Unfortunately, $\mathbf{V}$ cannot be obtained in a direct way.

Let $\hat{\boldsymbol{\eta}}_s$ be the ordinary least-square solution of (24). The corresponding residual vector can be expressed as

$$\boldsymbol{r}_s = \mathbf{Y} - \mathbf{X}\hat{\boldsymbol{\eta}}_s. \tag{26}$$

Considering the autoregressive model is often used to describe geophysical data [35] and the fourth difference is often used to monitor the noise level [36], it is feasible to assume $\boldsymbol{r}_s$ can be fit with the third-order autoregressive model as follows:

$$\boldsymbol{r}_s[k] = -f_1\boldsymbol{r}_s[k-1] - f_2\boldsymbol{r}_s[k-2] - f_3\boldsymbol{r}_s[k-3] + \boldsymbol{\epsilon}[k] \tag{27}$$

where the kth element of $\boldsymbol{r}_s$ is written as $\boldsymbol{r}_s[k]$, $f_i (i = 1, 2, 3)$ are the coefficients of the autoregressive model, and $\boldsymbol{\epsilon}$ denotes the white noise. A system of linear equation needs to be built according to (27) in order to determine the values of $f_i (i = 1, 2, 3)$.

By denoting the estimated value of f_i as $\hat{f}_i$, we can define a matrix as follows:

$$\mathbf{F} = \begin{pmatrix} \hat{f}_3 & \hat{f}_2 & \hat{f}_1 & 1 & 0 & \cdots & 0 \\ 0 & \hat{f}_3 & \hat{f}_2 & \hat{f}_1 & 1 & \cdots & 0 \\ \cdots & \cdots & \cdots & \ddots & \cdots & \cdots & 0 \\ 0 & \cdots & 0 & \hat{f}_3 & \hat{f}_2 & \hat{f}_1 & 1 \end{pmatrix}_{N-3,N} \tag{28}$$

and premultiply both sides of (24) by $\mathbf{F}$

$$\mathbf{FY} = \mathbf{FX}\boldsymbol{\eta} + \mathbf{F}\boldsymbol{\xi} = \mathbf{FX}\boldsymbol{\eta} + \tilde{\boldsymbol{\epsilon}} \tag{29}$$

where $\tilde{\boldsymbol{\epsilon}} \approx (\boldsymbol{\epsilon}[4], \boldsymbol{\epsilon}[5], \ldots, \boldsymbol{\epsilon}[N])^T$. At this point, the ultimate coefficient-estimating system is established. By taking $\tilde{\boldsymbol{\epsilon}}$ as the white noise approximately, we obtain the solution of (29) by using the ordinary least-square method and only then we arrive at the generalized least-square solution of (24)

$$\hat{\boldsymbol{\eta}}_{gls} = (\mathbf{X}^T\mathbf{F}^T\mathbf{FX})^{-1}\mathbf{X}^T\mathbf{F}^T\mathbf{FY}. \tag{30}$$

Considering the matrix $\mathbf{X}^T\mathbf{F}^T\mathbf{FX}$ in (30) might be singular or almost singular, a disturbance term can be introduced as follows:

$$\hat{\boldsymbol{\eta}}_{gr} = (\mathbf{X}^T\mathbf{F}^T\mathbf{FX} + \kappa\mathbf{I})^{-1}\mathbf{X}^T\mathbf{F}^T\mathbf{FY} \tag{31}$$

where $\mathbf{I}$ denotes a unit matrix, and $\kappa > 0$ is the so-called ridge parameter which is usually determined by the means of the generalized cross validation [37] and the *L-curve* [38].

IV. Simulation Study

A. Simulation and Test Method

In practice, not only the compensation system itself, but also many external factors, such as the quality of the installation on the aircraft, are crucial to the compensation result [39]. Since these external factors can be resolved with appropriate methods, it is feasible to exclude them temporarily. Therefore, numerical simulation data sets are employed here. The simulation takes advantage of FlightGear [40] and WMM2015 [41]. For more details about the simulation (see [30]).

The coefficients of the Tolles–Lawson model should be estimated and tested separately. Thus, two sets of calibration flights are essential for recording the scalar and vector magnetic field data. The coefficients of the Tolles–Lawson model can be estimated using the data recorded during the first calibration flight and then applied to the second calibration flight to calculate and remove the aircraft magnetic interference in real time. The standard deviation of the residual interference in the compensated signal can be used to evaluate the accuracy of the estimated coefficients [31].

The passband of *bpf* is set from 0.06 to 0.6 Hz [17], where it is supposed to be the primary frequency range of the aircraft interference. Since the Gaussian filter is recommended in [26], the bandpass filter *bpf* is implemented as the cascade of a Gaussian high-pass filter and a Gaussian low-pass filter. The ridge parameter κ is determined by the means of the *L-curve* proposed in [38]. The estimator (31) is adopted to estimate the coefficients.

B. Result and Analysis

Our investigation starts out from (6). For an ideal three-axis strapdown magnetometer, $\mathbf{C}$ and $\boldsymbol{l}$ in (6) can be given by

$$\mathbf{C} = \begin{pmatrix} 1 & 0 & 0 \\ 0 & 1 & 0 \\ 0 & 0 & 1 \end{pmatrix} \quad \boldsymbol{l} = \begin{pmatrix} 0 \\ 0 \\ 0 \end{pmatrix}. \tag{32}$$

It should be emphasized that herein the Gaussian white noise $\boldsymbol{n}$ has always been included in the test data. Since the deviations from (32) are practically inevitable, we can rewrite (32) as

$$\mathbf{C} = \begin{pmatrix} 1+c_{11} & c_{12} & c_{13} \\ c_{21} & 1+c_{22} & c_{23} \\ c_{31} & c_{32} & 1+c_{33} \end{pmatrix} \quad \boldsymbol{l} = \begin{pmatrix} l_1 \\ l_2 \\ l_3 \end{pmatrix} \tag{33}$$

where c_{ij} and l_i $(i = 1, 2, 3;\ j = 1, 2, 3)$ denote the deviations caused by the three-axis magnetometer. From (6) and (33), it can be derived that c_{ij} indicates the effects from the jth component of the three-axis magnetometer on its ith one. The influences of c_{ij} or l_i can be studied separately by changing its value gradually and meanwhile setting the others to 0. Fig. 2 shows the corresponding standard deviations of the residual interferences which are, respectively, obtained with the classical Tolles–Lawson model and the modified one.

As can be seen in Fig. 2, for the classical Tolles–Lawson model, the standard deviation of the residual interference

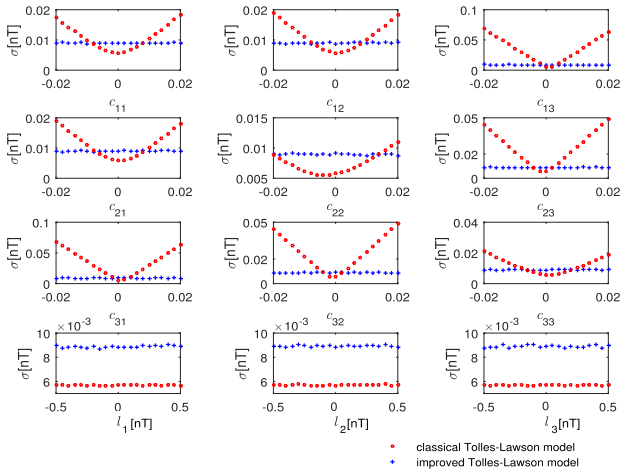

Fig. 2. Standard deviation σ of the residual interference when only c_{ij} or l_i is set to a nonzero value and meanwhile the others are set to 0. The value ranges of c_{ij} and l_i in this simulation are chosen empirically.

varies apparently when c_{ij} takes values in the range from -0.02 to 0.02; with c_{ij} getting close to 0, the standard deviation becomes smaller and approaches the minimum value. This demonstrates that the classical Tolles–Lawson model is sensitive to these errors of the three-axis strapdown magnetometer reflected by $\mathbf{C}$. Note that for cases c_{13}, c_{23}, c_{31}, c_{32}, and c_{33} (all of which involve the third component of the three-axis magnetometer, corresponding to the **z**-axis), the range of values taken by the standard deviations is larger than for cases c_{11}, c_{12}, c_{21}, and c_{22}. As mentioned in [11], the aircraft cannot alter the dip angle so that the collected data corresponding to the **z**-axis is incomplete. Therefore, the results are more sensitive to the third component of the three-axis magnetometer.

For the modified Tolles–Lawson model, the standard deviation of the residual interference remains much more stable, regardless of the varying c_{ij}'s. Although in the cases c_{13}, c_{23}, c_{31}, c_{32}, and c_{33}, the standard deviations take smaller values for the modified Tolles–Lawson model in almost the entire range, it no longer holds for the rest of the cases. When c_{11}, c_{12}, c_{21}, and c_{22} get closer to 0, the standard deviations take smaller values for the classical Tolles–Lawson model. For the cases l_i's, both models are able to yield stable results, but the classical one can produce a better result. Considering the only difference in such cases is whether λ is introduced, it can be inferred from (9) that the noise $\boldsymbol{n}$ will play a major role in determining λ if c_{ij} or l_i reaches to a certain small enough value, thus leading to the disturbance of λ and bringing on side effects to the estimation of the coefficients. As a result, the standard deviations for the modified Tolles–Lawson model maintain their values at about 0.01 nT for all the cases.

As shown in Fig. 3, where all c_{ij}'s are simultaneously set to ω and l_i's to 25 times ω, the classical Tolles–Lawson model can perform fairly well when the measurement errors of the three-axis strapdown magnetometer are minimal, but the modified one is more robust to larger measurement errors. It should be noted that for the classical model, the result of combined effects of all c_{ij} and l_i is not a simple straightforward superposition of the results in Fig. 2. This can be

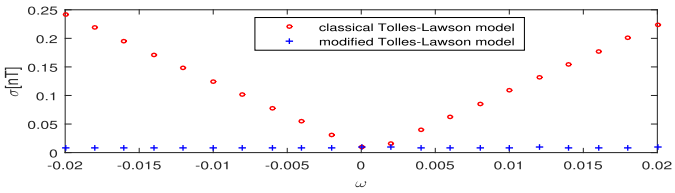

Fig. 3. Standard deviation σ of the residual interference when all c_{ij}'s are set to ω and meanwhile l_i's are set to 25 times ω.

attributed to the quadratic terms of the direction cosines and their derivatives in the model, and the characteristics of the equations used to estimate the coefficients are changed with the direction cosines. It can be inferred from Fig. 3 that the modified model is recommended when the three-axis strapdown magnetometer has a larger measurement error.

V. Discussion

The modified Tolles–Lawson model is illustrated to be a reliable alternative when the adopted three-axis strapdown magnetometer has a fairly low measurement accuracy. From the view of the Tolles–Lawson model, the balance between the two sides of the equations would be broken by not only the different measuring performances of the scalar and vector magnetometers themselves but also some external factors, such as their different mounting positions, which deserves to be studied in the future.

References

[1] M. S. Reford and J. S. Sumner, "Aeromagnetics," *Geophysics*, vol. 29, no. 1, pp. 482–516, Aug. 1964.

[2] M. N. Nabighian *et al.*, "The historical development of the magnetic method in exploration," *Geophysics*, vol. 70, no. 6, pp. 33ND–61ND, 2005.

[3] P. J. Hood, "History of aeromagnetic surveying in Canada," *Lead. Edge*, vol. 26, no. 11, pp. 1384–1392, Nov. 2007.

[4] P. Leliak, "Identification and evaluation of magnetic-field sources of magnetic airborne detector equipped aircraft," *IRE Trans. Aerosp. Navigat. Electron.*, vol. ANE-8, no. 3, pp. 95–105, Sep. 1961.

[5] H. Dong and C. Zhang, "A further review of the quantum magnetometers," *Chin. J. Eng. Geophys.*, vol. 7, no. 4, pp. 460–470, Aug. 2010.

[6] J. F. Vasconcelos, G. Elkaim, C. Silvestre, P. Oliveira, and B. Cardeira, "Geometric approach to strapdown magnetometer calibration in sensor frame," *IEEE Trans. Aerosp. Electron. Syst.*, vol. 47, no. 2, pp. 1293–1306, Apr. 2011.

[7] Y. X. Liu *et al.*, "Novel calibration algorithm for a three-axis strapdown magnetometer," *Sensors*, vol. 14, no. 5, pp. 8485–8504, 2014.

[8] M. Wołoszyn, "Analysis of aircraft magnetic interference," *Int. J. Appl. Electromagn. Mech.*, vol. 39, nos. 1–4, pp. 129–136, 2012.

[9] G. Noriega, "Model stability and robustness in aeromagnetic compensation," *First Break*, vol. 31, no. 3, pp. 73–79, Mar. 2013.

[10] P. M. Williams, "Aeromagnetic compensation using neural networks," *Neural Comput. Appl.*, vol. 1, no. 3, pp. 207–214, Sep. 1993.

[11] S. H. Bickel, "Small signal compensation of magnetic fields resulting from aircraft maneuvers," *IEEE Trans. Aerosp. Electron. Syst.*, vol. AES-15, no. 4, pp. 518–525, Jul. 1979.

[12] S. H. Bickel, "Error analysis of an algorithm for magnetic compensation of aircraft," *IEEE Trans. Aerosp. Electron. Syst.*, vols. AES–15, no. 5, pp. 620–626, Sep. 1979.

[13] B. W. Leach, "Automatic aeromagnetic compensation," Nat. Aeronaut. Lab., Nat. Res. Council Canada, Ottawa, ON, Canada, Tech. Rep. LTR-FR69, Mar. 1979.

[14] B. W. Leach, "Aeromagnetic compensation as a linear regression problem," in *Information Linkage Between Applied Mathematics and Industry II*. New York, NY, USA: Academic, 1979, pp. 129–161.

[15] P. Deng, C. Lin, B. Tan, and J. Zhang, "Application of adaptive filtering algorithm based on wavelet transformation in aeromagnetic survey," in *Proc. IEEE 2nd Int. Conf. Comput. Sci. Inf. Technol.*, Chengdu, China, Jul. 2010, pp. 492–496.

[16] J. Zhang, C. Lin, and W. Lin, "An improved c-k class estimation of the regression parameters in aircraft magnetic interference model," in *Proc. CINC*, Wuhan, China, 2010, pp. 103–106.

[17] B. Gu, Q. Li, and H. Liu, "Aeromagnetic compensation based on truncated singular value decomposition with an improved parameter-choice algorithm," in *Proc. CISP*, Hangzhou, China, 2013, pp. 1545–1551.

[18] Z. Dou *et al.*, "An adaptive filter for aeromagnetic compensation based on wavelet multiresolution analysis," *IEEE Geosci. Remote Sens. Lett.*, vol. 13, no. 8, pp. 1069–1073, May 2016.

[19] Y. Zhang, Y. X. Zhao, and S. Chang, "An aeromagnetic compensation algorithm for aircraft based on fuzzy adaptive Kalman filter," *J. Appl. Math.*, vol. 2014, Aug. 2014, Art. no. 405671.

[20] C. Lin, J.-J. Zhou, and Z.-Y. Yang, "A method to solve the aircraft magnetic field model basing on geomagnetic environment simulation," *J. Magn. Magn. Mater.*, vol. 384, pp. 314–319, Jun. 2015.

[21] C. D. Hardwick, "Important design considerations for inboard airborne magnetic gradiometers," *Geophysics*, vol. 49, no. 11, pp. 2004–2018, Nov. 1984.

[22] J. B. Nelson, "An improved aeromagnetic data acquisition system for the NRC Convair 580," Nat. Res. Council Canada, Inst. Aerosp. Res., Ottawa, ON, Canada, Tech. Rep. LTR-FR-170, Nov. 2000.

[23] J. B. Nelson, "Aeromagnetic noise from magnetometers and data acquisition systems," presented at the 8th Int. Congr. Brazilian Geophys. Soc., Rio de Janeiro, Brazil, 2003.

[24] J. Jia, R. Groom, and B. Lo, "The use of GPS sensors and numerical improvements in aeromagnetic compensation," presented at the Annu. Meeting Soc. Exploration Geophys. (SEG), Denver, CO, USA, 2004.

[25] J. Jia, B. Lo, and R. Groom, "Final report on improved aeromagnetic compensation for OMET program," Ontario Mineral Exploration Technol. Program, Ottawa, ON, Canada, Tech. Rep. Project P02-03-043, May 2004.

[26] R. W. Groom, R. Jia, and B. Lo, "Magnetic compensation of magnetic noises related to aircraft's maneuvers in airborne survey," presented at the 17th EEGS Symp. Appl. Geophys. Eng. Environ. Problems, Ottawa, ON, Canada, 2004.

[27] B. Zhang, Z. Qiao, and Y. Qiao, "A simplified aeromagnetic compensation model for low magnetism UAV platform," in *Proc. IEEE Int. Geosci. Remote Sens. Symp.*, Vancouver, BC, Canada, Jul. 2011, pp. 3401–3404.

[28] R. M. Caron, C. Samson, P. Straznicky, and S. Ferguson, "Aeromagnetic surveying using a simulated unmanned aircraft system," *Geophys. Prospecting*, vol. 62, no. 2, pp. 352–363, 2014.

[29] Z. Liu, H. Pang, M. Pan, and C. Wan, "Calibration and compensation of geomagnetic vector measurement system and improvement of magnetic anomaly detection," *IEEE Geosci. Remote Sens. Lett.*, vol. 13, no. 3, pp. 447–451, Mar. 2016.

[30] Z. Dou *et al.*, "An aeromagnetic compensation coefficient-estimating method robust to geomagnetic gradient," *IEEE Geosci. Remote Sens. Lett.*, vol. 13, no. 5, pp. 611–615, May 2016.

[31] G. Noriega, "Performance measures in aeromagnetic compensation," *Lead. Edge*, vol. 30, no. 10, pp. 1122–1127, Oct. 2011.

[32] K. Levenberg, "A method for the solution of certain non-linear problems in least squares," *Quart. J. Appl. Math.*, vol. 2, no. 2, pp. 164–168, Jul. 1944.

[33] A. N. Tikhonov and V. Y. Arsenin, *Solutions of Ill-Posed Problems*. Hoboken, NJ, USA: Wiley, 1977.

[34] M. S. Zhdanov, *Inverse Theory and Applications in Geophysics*. New York, NY, USA: Elsevier, 2015.

[35] M. E. Greotski, O. Jensen, and J. Arkani-Hamed, "Fractal stochastic modeling of aeromagnetic data," *Geophysics*, vol. 56, no. 11, pp. 1706–1715, Nov. 1991.

[36] C. Reeves, "Aeromagnetic surveys principles, practice & interpretation," in *Proc. GEOSOFT*, Oct. 2005, p. 42.

[37] G. H. Golub, M. Heath, and G. Wahba, "Generalized cross-validation as a method for choosing a good ridge parameter," *Technometrics*, vol. 21, no. 2, pp. 215–223, May 1979.

[38] P. C. Hansen, "Analysis of discrete ill-posed problems by means of the L-curve," *SIAM Rev.*, vol. 34, no. 4, pp. 561–580, Dec. 1992.

[39] G. Noriega, "Aeromagnetic compensation in gradiometry—Performance, model stability, and robustness," *IEEE Geosci. Remote Sens. Lett.*, vol. 12, no. 1, pp. 117–121, Jan. 2015.

[40] Gijs, Amsterdam, the Netherlands. (May 2010). *Professional and Educational FlightGear Users*. [Online]. Available: http://wiki.flightgear.org/Professional_and_educational_FlightGear_users.

[41] A. Chulliat *et al.*, "The US/UK world magnetic model for 2015–2020," NOAA, Boulder, CO, USA, Tech. Rep. NESDIS/NGDC, 2015.